Exfoliation and Restacking of Lepidocrocite-type Layered Titanates Studied by Small-Angle X-ray Scattering

Rogier Besselink,[†] Tomasz M. Stawski,[†] Hessel L. Castricum,[‡] Dave H. A. Blank,[†] and Johan E. ten Elshof*,[†]

MESA$^+$ Institute for Nanotechnology, University of Twente, P.O. Box 217, 7500 AE Enschede, The Netherlands, and Van't Hoff Institute for Molecular Sciences, University of Amsterdam, 1018 WV, Amsterdam, The Netherlands

Received: September 12, 2010; Revised Manuscript Received: November 2, 2010

The exfoliation of the lepidocrocite-type layered titanate $K_{0.8}[Ti_{1.73}Li_{0.27}O_4]$ (KLTO) in aqueous solution and the restacking of exfoliated nanosheets was investigated by small-angle X-ray scattering (SAXS). Suspensions with completely exfoliated titania nanosheets of 1 nm thickness were obtained after protonation of KLTO to $HTi_{1.6}O_{3.7}$ (HTO), followed by addition of tetrabutyl ammonium hydroxide (TBAOH) to a molar ratio TBAOH/HTO = 1. Restacking of nanosheets into small stacks of 2−4 units occurred at TBAOH/HTO ratios of 1.6 or higher. The separation distance between the sheets was found to be reversible and very sensitive to the pH and ionic strength of the solution and increased up to 12 nm. The experimental data indicate that the separation distance between restacked nanosheets scaled with the Debye length of the solution. This suggests that the stacks are organized via electrostatic interactions due to the presence of a diffuse double layer of positively charged ions between the negatively charged nanosheets.

1. Introduction

Nanosheets of various materials have drawn much attention in recent years as they constitute truly two-dimensional building blocks that can be used to fabricate electronic devices with enhanced properties.[1,2] These systems exhibit extremely high anisotropy in the vertical direction in comparison with their lateral dimensions (ca. 1 nm thickness versus 1 μm in lateral directions). The research in this field was also stimulated by the successful separation and characterization of a single sheet of graphite known as graphene.[3] It has become clear that nanosheets of exfoliated layered oxides may open up new roads in nanoelectronics and solid state research. For instance, thin film assemblies composed of titanium oxide nanosheets were reported to exhibit very high dielectric constants,[4−6] and titanium oxide nanosheets doped with Co proved to be ferromagnetic.[7] Even multicomponent devices with a p−n junction that exploit the photoelectric effect have been fabricated from nanosheets, as in the case of devices made from exfoliated niobate $[(CH_3)_3NHSr_2Nb_3O_{10}]$ and synthetic saponite $(Na_{0.96}[Si_{7.18}-Al_{0.64}]Zn_{6.20}O_{20}(OH)_2)$ crystals.[8]

Typically, the layered oxide crystals that are precursors for the synthesis of nanosheets are often based on the layered oxides of titanium (Ti), manganese (Mn), or niobium (Nb), as well as on layered perovskites such as $LaNb_2O_7$. A common technique of fabrication of nanosheets is the delamination of layered crystals by intercalation with bulky ions such as tetrabutylammonium cations (TBA^+). The exfoliation process is slow and reversible to some extent.[4,9] Titanium oxide nanosheets have been made using this technique by exfoliation of lepidocrocite-like crystals of $A_xTi_{2-x/3}Li_{x/3}O_4$ (where A is K, Rb, or Cs)[10] using tetrabutylammonium hydroxide as a source of bulky TBA^+ spacers.[11] Following exfoliation, the controlled restacking and reassembly of the negatively charged titania nanosheets is one of the key issues in the processing of this material into functional films. For instance, thin films of nanosheets were made via layer-by-layer deposition of polycations and titania nanosheets,[12] which is in fact a process of controlled restacking of sheets. Hence, detailed information concerning the kinetics of the exfoliation process, and the structure of the material during the exfoliation process, is of high relevance.

In the present study, small-angle X-ray scattering (SAXS) was employed to study the structure and structural evolution of exfoliating titania nanosheets from a lepidocrocite-type titanate crystal $K_{0.8}[Ti_{1.73}Li_{0.27}O_4]$, and the restacking of individual sheets by varying the TBA^+ concentration, pH, and the ionic strength of the solution. The presence of pseudo-Bragg peaks in the SAXS curves indicates the presence of stacked nanosheets. As will be shown below, the formation of TBA^+/nanosheet stacks is very a dynamic process, and the extent of stack formation depends strongly on both ionic strength and the type of cations present in solution.

To interpret the scattering data, we employed the Fluctuating Gap Model developed by Pizzey et al. to describe the scattering of suspensions of colloidal plates in a nematic liquid crystal.[13] The model was originally developed for the characterization of clay particles, but is also applicable to the colloidal nanosheet solutions under investigation here. According to this model, the scattering intensity $I(q)$ of isotropically dispersed stacks of two-dimensional planes as a function of the scattering vector q is given by the expression:

* Corresponding author. Tel.: +31 53 489 2695. Fax: +31 53 489 2990. E-mail: j.e.tenelshof@utwente.nl.
[†] University of Twente.
[‡] University of Amsterdam.

10.1021/jp108687q
Published on Web 11/23/2010

$$I(q) \approx \frac{S}{q^2}\left(\frac{\sin(^{q\cdot h}/_2)}{(^{q\cdot h}/_2)}\right)^2 \cdot \left[(x\cdot \sin^2(^{q\cdot d}/_2) + (1-x)\cdot\langle \sin^2(^{m\cdot q\cdot d}/_2)\rangle_{\mu,\sigma})\cdot\left(\frac{1}{\sin(^{q\cdot d}/_2)} - \frac{\phi}{(^{q\cdot d}/_2)}\right)^2\right] \quad (1)$$

Here, h is the thickness of the plate, and d is the spacing between two plates/sheets in the crystal or in a stack of sheets. The parameter x refers to the fraction of sheets that is isolated in solution, so that $(1 - x)$ refers to the fraction of nanosheets that is part of some stack of sheets. The parameter ϕ is used to adjust the electron density of the surroundings of any stack of plates. In very dilute suspensions, the electron density of the surroundings of a stack of sheets has the same electron density as the solvent ($\phi = 0$). However, in concentrated suspensions, a stack of sheets is surrounded by a large number randomly oriented particles (stacks of sheets). This lowers the contrast in electron density between stacks of sheets and their surroundings and therefore lowers the zero-order pseudo-Bragg peak with respect to the higher order Bragg-peaks. In case that $\phi = 1$, the electron density of the surroundings equals the electron density of a stack of sheets and the zero-order pseudo-Bragg peak disappears completely.

A distribution of stack number m was introduced to obtain a suitable model that describes the broad pseudo-Bragg peaks. In this model, the distribution is described by a Gaussian distribution $\rho(m,\mu,\sigma)$, which has a maximum at $m = \mu$ and a standard deviation σ. The term $\langle \sin^2(mqd/2)\rangle$ in eq 1 is a weighted average of the contribution of all stacks with different stack number m and is defined as:

$$\langle \sin^2(m\cdot q\cdot d/2)\rangle = \frac{\sum_{m=2}^{\max} \rho(m,\mu,\sigma)\cdot \sin^2(^{m\cdot q\cdot d}/_2)}{\sum_{m=2}^{\max} \rho(m,\mu,\sigma)} \quad (2)$$

Analogous to the $\langle \sin^2(mqd/2)\rangle$ term, the average number of sheets in a single stack of sheets, hereafter referred to as the averaged stack number $\langle m\rangle$, is a weighted average that is defined by eq 3. Both the weighted average $\langle m\rangle$ and $\langle \sin^2(mqd/2)\rangle$ were only evaluated for realistic stack numbers ($m \geq 2$).

$$\langle m\rangle = \frac{\sum_{m=2}^{\max} \rho(m,\mu,\sigma)\cdot m}{\sum_{m=2}^{\max} \rho(m,\mu,\sigma)} \quad (3)$$

2. Experimental Section

2.1. Synthesis of Titania Nanosheets. The method developed by Tanaka et al.[11] was used for the preparation of titania nanosheets. Plate-like $K_{0.8}Ti_{1.73}Li_{0.27}O_4$ (KLTO) crystals were formed in a flux of potassium molybdate at elevated temperatures between 1000 and 1100 °C. The reactants TiO_2 (Riedel-de Haen, 99%), K_2CO_3 (Fluka, 99%), Li_2CO_3 (Riedel-de Haen, 99%), and MoO_3 (Sigma-Aldrich, 99.5%) powders were weighed in a platinum crucible in molar ratios of 1.73:1.67:0.13:1.27 and then heated. MoO_3 and excess K_2CO_3 form a liquid flux at elevated temperature, promoting the growth of the KLTO crystals during synthesis.

TABLE 1: Concentrations of the Analyzed Suspensions[a]

titration with TBAOH (aq)				titration with HNO_3			dilution with H_2O		
Nr	TBA/HTO[b]	C_{HTO}[c]	pH	Nr	C_{HTO}[c]	pH	Nr	C_{HTO}[c]	pH
T0	1.0	5.0	12.5	N0	3.0	12.7	D0	3.0	12.7
T1	2.0	4.0	12.5	N1	3.0	12.7	D1	2.7	12.6
T2	2.3	3.8	12.6	N2	3.0	12.7	D2	2.4	12.6
T3	2.7	3.5	12.6	N3	2.9	12.7	D3	2.1	12.5
T4	3.3	3.3	12.6	N4	2.9	12.6	D4	1.8	12.4
T5	3.7	3.0	12.7	N5	2.8	12.5			
T6	5.0	2.5	12.8	N6	2.6	12.4			
T7	7.0	2.0	12.9						

[a] Samples T0−T7 refer to sample T0 after titration with tetrabethyl ammonium hydroxide. Samples N0−N6 refer to sample T5 after titration with nitric acid. Samples D0−D4 refer to sample T5 after dilution with doubly distilled water. [b] The TBA/HTO ratio is defined as the ratio beween TBA^+ and all exchangeable protons of HTO. [c] C_{HTO} = the equivalent concentration of $H_1Ti_{1.6}O_{3.7}\cdot 0.93H_2O$ crystals (g/L).

The final KLTO crystals were washed in 500 mL of a nitric acid solution (2 mol/L) for more than 5 days to exchange K^+ and Li^+ by H^+. The nitric acid solution was renewed five times by decantation. Next, the mixture was filtered and washed three times with water. Suspensions containing 5 g/L HTO ($H_1Ti_{1.6}O_{3.7}\cdot 0.93H_2O$) and a 1:1 molar ratio of tetrabutyl ammonium hydroxide (TBAOH) versus exchangeable protons of HTO, that is, TBA/HTO = 1.0, were used as starting point in the experiments (sample T0). The material was completely dispersed in the solution, and the solution was stable for at least 3 weeks.

The effect of the TBA/HTO ratio was investigated by titration of the above-mentioned suspension either with a TBAOH solution of 130 mmol/L or with a nitric acid solution of 500 mmol/L. These two series of samples are designated in Table 1 with the letters T and N, respectively. The effect of ionic strength was investigated independently by diluting a restacked suspension with doubly distilled water. These samples are designated in Table 1 with the letter D.

2.2. SAXS Experiments. The colloidal samples were placed in capillary glass tubes (Hilgenberg, dimensions: 80 mm length; 1.5 mm diameter; wall thickness ~10 μm). Small-angle X-ray scattering was carried out using synchrotron radiation on the Dutch-Belgian beamline, DUBBLE BM-26B of the ESRF in Grenoble.[14] The X-ray beam with an energy of 16 keV was focused on a corner of the 2D gas-filled multiwire proportional gas-filled detector to maximize the covered range of scattering angles. A beam stop was applied to shield the detector from the direct beam and avoid saturation of the outgoing signal. The detector was placed at a distance of 1.5 m from the sample, which allowed us to obtain data in the range $0.44 < q < 8.00$ nm^{-1}. All scattering data were found to be independent of the scattering angle φ in the plane of the detector. As this indicates that the samples were isotropically dispersed, the measured intensities from all channels with the same q value were averaged. Silver behenate was used as the calibration standard for the determination of the absolute scale of the scattering vector q in our experiments.[15]

The scattering intensity of the capillary containing a given colloidal sample was collected as a function of scattering vector q. All curves were normalized by dividing the scattering intensity by both the time of data acquisition and the total intensity of the scattered signal measured by an ion chamber placed immediately behind the sample. A background subtraction procedure was carried out using the signal of a capillary that contained water as background.

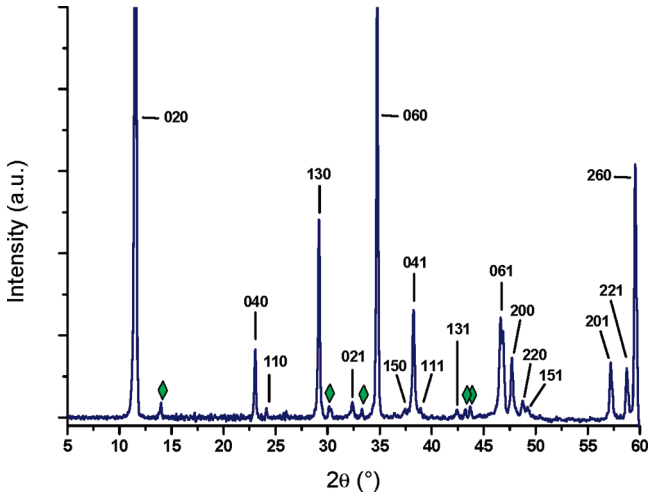

Figure 1. XRD pattern of lepidocrocite-type $K_{0.80}Ti_{1.73}Li_{0.27}O_4$ phase. Numbers indicate respective *hkl* values of the lepidocrocite peaks, and "◇" denotes diffraction peaks of potassium hexatitanate.

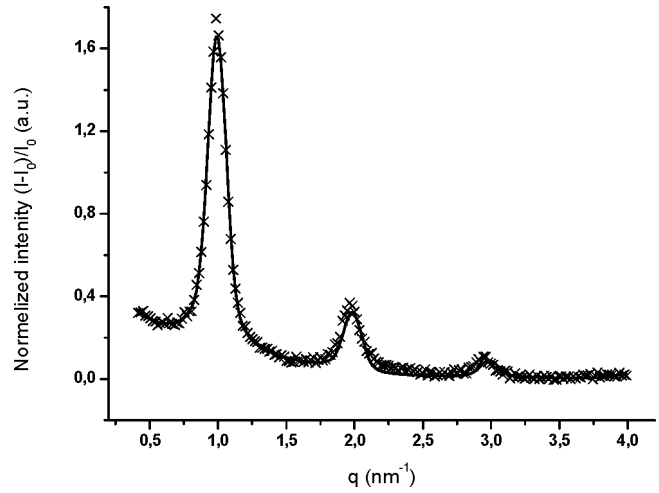

Figure 3. Experimental and fitted scattering curve of sample T7 with TBA/HTO = 7.0. The "×" marks indicate the experimental data. The drawn line indicates the best fit of the Fluctuating Gap Model to the experimental data.

2.3. XRD Experiments. X-ray diffraction (XRD) was carried out on a Philips diffractometer PW3020 (Software XPert Data Collector 2.0e, Panalytical B.V., Almelo, The Netherlands) using Cu K_α radiation.

2.4. AFM Experiments. Contact-mode atomic force microscopy was used to measure the thickness of single nanosheets. Therefore, the pH of a nanosheets suspension (2 g/L HTO) was reduced to pH 7 by titration with hydrochloric acid (1 mol/L, prepared from 37% hydrochloric acid, Acros Organics). Large particles were removed with a Hereas Biofruge Primo centrifuge at 5000 rpm. Subsequently, nanosheets were deposited by immersion of sapphire substrates (Al_2O_3, 0.5 × 10 × 10 mm, SurfaceNet GmbH, Germany) with exposed (11$\underline{2}$0) surface in the nanosheet suspension. The substrate was then washed with both water and ethanol, and AFM measurements carried out on a Veeco Nanoscope III.

3. Results and Discussion

3.1. XRD Analysis. The XRD pattern of flux-grown particles in Figure 1 is in agreement with the lepidocrocite-type structure of $K_{0.8}Ti_{1.73}Li_{0.27}O_4$.[11] A few other low intensity diffraction peaks were assigned to potassium hexatitanate ($K_2Ti_6O_{13}$, JCPDS: 40-0403), the formation of which may have been caused by a small deficiency of lithium due to evaporation of lithium oxide (BP = 1155 °C).

3.2. AFM Imaging. The contact mode height image in Figure 2 reveals the presence of very thin platelets on a sapphire substrate after deposition of nanosheets. The thickness of these nanosheets lies in the range between 0.8 and 1.3 nm, and the lateral dimensions of the nanosheets are in the range between 50 and 300 nm. The platelets seem to have a rough morphology, which may be due to the presence of a residual quarternary ammonium ion layer, but it is also possible that the flexible sheets have creased to some extent on the surface. The measurement enabled us to determine the dimensions of a single sheet, and the values are in good agreement with data from literature.[4]

3.3. Evaluation of the Fluctuating Gap Model. Most scattering curves discussed in this study contain pseudo-Bragg peaks, which indicate the presence of regularity within the various colloidal solutions of the layered HTO system $H_1Ti_{1.6}O_{3.7}$. A typical example is sample T7 shown in Figure 3. The higher-order pseudo-Bragg peaks are located exactly at integer number of times the position of the first-order pseudo-

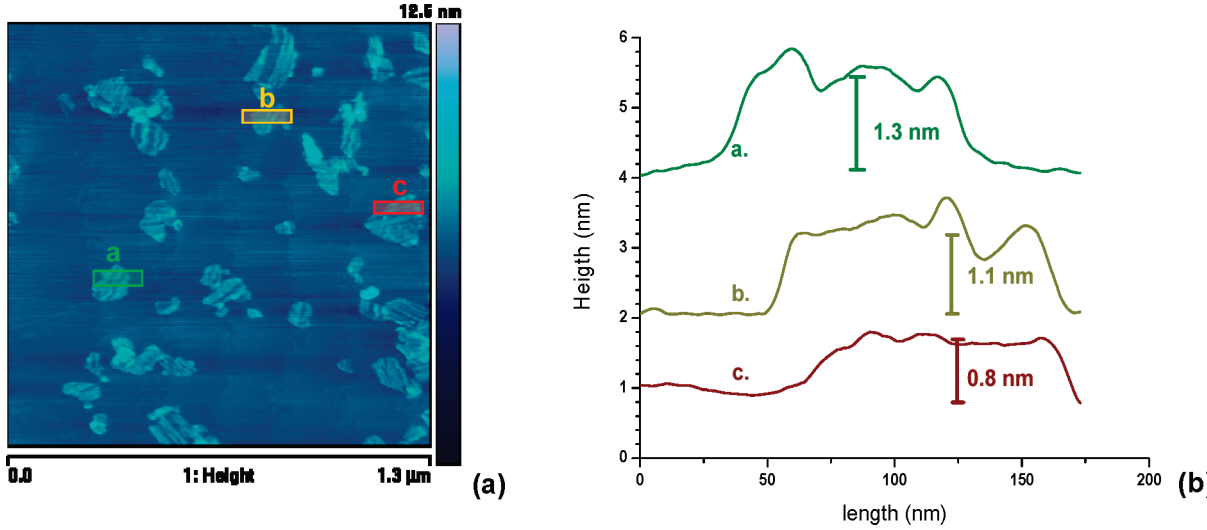

Figure 2. AFM height image of titania nanosheets deposited on a sapphire substrate: (a) height image; (b) height profiles of selected sections that correspond to the indicated regions in the height image.

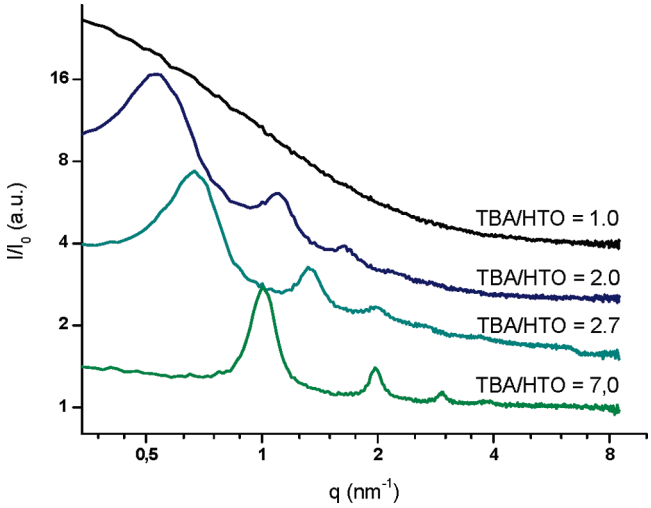

Figure 4. Small-angle scattering curve of colloidal suspensions with different TBA/HTO ratios, where TBA/HTO = [TBA]/[$H_1Ti_{1.6}O_{3.7}$].

Bragg peaks, that is, $q_{00n} = n \cdot q_{001}$, with n an integer value. This type of scattering curve agrees with a system consisting of one-dimensional stacks of either rod-shaped or disk-shaped entities.[16] Moreover, only small deviations were found between the widths of first and higher order pseudo-Bragg peaks. We may therefore neglect distorted reflections that arise from deviations of the intervening space between stacked particles, as described by the Babinet component in the Fluctuating Gap Model.[16] The pseudo-Bragg peaks can therefore be solely described in terms of undistorted crystalline reflections, and peak broadening was predominantly caused by the limited length scale over which internal order was present. The Fluctuating Gap Model was fitted to the experimental data. On the basis of the data from AFM analysis (Figure 2), the thickness of nanosheets h was in all cases set to 1.0 nm.[4] Because the number of data points that describes a single pseudo-Bragg peak is limited to ~20, it was not possible to determine the standard deviation σ of the Gaussian that describes the stack size distribution accurately. However, as discussed in more detail in the Supporting Information, the standard deviation has only a very minor influence on the shape of the pseudo-Bragg peaks. Values of σ larger than 2 were adopted in the calculations, and the maximum stack size m_{max} was set to 8, as explained in the Supporting Information. The five parameters μ, ϕ, d, x, and S were then fitted as independent variables to the experimental curves.

3.4. Titration of HTO with TBAOH and HNO_3. Figure 4 shows a series of scattering curves of HTO suspensions T0, T1, T3, and T7. The scattering curve of T0 (TBA^+/HTO = 1.0) is characteristic for randomly oriented scattering objects with a finite size. No pseudo-Bragg peaks are present in the curve. This indicates the absence of internal crystallographic order in the suspension and proves that the HTO crystals were completely exfoliated into two-dimensional nanosheets $(Ti_{1.73}O_4)^{\delta-}$ in sample T0. These findings are in close agreement with data of Tanaka et al., who reported complete exfoliation of the same HTO compound under similar conditions.[11] When TBAOH was added to this suspension until TBA^+/HTO = 2.0, broad pseudo-Bragg peaks appeared. This indicates some degree of restacking of two-dimensional sheets into ordered three-dimensional objects. Further increase of the TBA^+/HTO ratio involved a shift of all pseudo-Bragg peaks toward higher q-values, as is shown in Figure 4 for samples T3 and T7. The suspensions samples with the highest ratios were not completely stable, and slow flocculation was observed. However, they were stable for more than an hour, which exceeds the sample measurement time of ~5 min by far. The observed shift of the pseudo-Bragg peaks toward higher q-values indicates a reduction of the separation distance between the nanosheets with increasing TBA^+ concentration. Furthermore, the peak width decreased with the addition of TBA^+. Especially sample T7 is considerably narrower than T1 and T3, which indicates the occurrence of internal order in the restacked systems on a longer length scale.

Fitting of the Fluctuating Gap Model to the scattering curves of samples T0−T7 and N1−N6 yielded values for the separation distance d between restacked $Ti_{1.73}O_4$ nanosheets, the average stack number $\langle m \rangle$, and the fraction of exfoliated nanosheets x. The trends are shown in Figure 5. The ratio TBA^+/H^+ is based on the added amount of TBAOH and the actual pH of the solution. Addition of TBAOH to sample T0 led to a gradual decrease in the separation distance between sheets from 12 to 6 nm, and an increase of the average stack size from 2.5 to 4.1 (±0.3) nanosheets. The trend in the fraction of exfoliated nanosheets x in Figure 5c is less pronounced, but shows an overall gradual decrease with increasing TBAOH concentration.

These titration experiments demonstrate that completely exfoliated nanosheets are obtained at a TBA/HTO ratio of unity, where all exchangeable protons from HTO have been neutralized by OH^- from TBAOH, and have effectively been replaced by TBA^+, that is:

$$HTi_{1.6}O_{3.7} + TBAOH \rightarrow (TBA)Ti_{1.6}O_{3.7} + H_2O$$

When the TBA^+ concentration was increased further, restacking occurred. Restacking is driven by attractive electrostatic interactions between the nanosheets. The magnitude and overall trend observed in the interlayer spacings are in good agreement with the reported interlayer spacings of HTO crystals due to osmotic swelling reported by Tanaka et al.[11] Although swelling of HTO crystals and the restacking of nanosheets are different processes, the final result may be structurally similar. This explains the similarity in the interlayer spacing at similar TBA/HTO ratio in the two cases and suggests that a thermodynamically stable structure evolves.

A complete reversal of the trend was observed upon addition of nitric acid. The decrease of the TBA^+/H^+ ratio led to an increase in separation distance and a decrease of average stack number, and the optimized parameters were very similar for similar TBA^+/H^+ ratios. This is another indication of a dynamic and reversible process close to equilibrium conditions. In agreement with expectation, the increase of interlayer spacing upon titration cannot be explained by the mere effect of dilution, because the observed increase was at least 3 times larger than is predicted by the volumetric increase due to the addition of titration solution.

The total number of ions in solution maintained constant in the experiments where nitric acid was added, because the excess of hydroxyl anions in solution were neutralized by protons and effectively replaced by nitrate ions. This shows that the interlayer distance between the titanate planes in the stacks is not determined only by the ionic strength of the solution, but also correlates with the molar ratio TBA^+/H^+, and therefore with the pH of the solution. Titration of nitric acid below pH 12 led to rapid precipitation of HTO crystallites. No intermediate states between completely exfoliated nanosheets and HTO-crystallites could be observed with SAXS in that case. Because H^+ can probably have a more effective electrostatic interaction with nanosheets than TBA^+ due to its smaller size, it is possible that

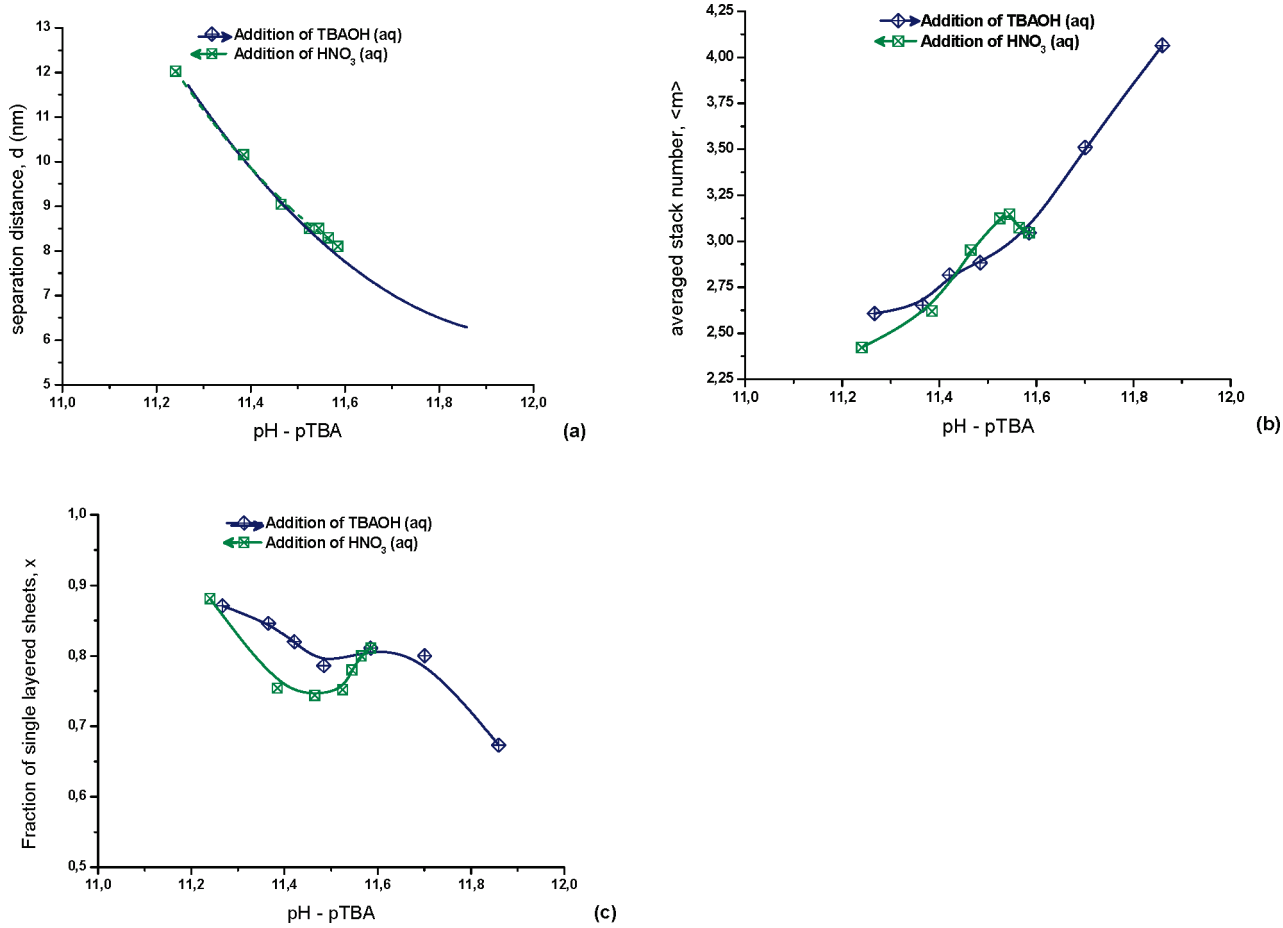

Figure 5. Stacking parameters d, $\langle m \rangle$, and x of the Fluctuating Gap Model as a function of the difference between the measured pH and calculated pTBA (−log[TBAOH]): (a) separation distance between platelets d; (b) average stack number $\langle m \rangle$; and (c) fraction of single nanosheets x.

the addition of protons from HNO_3 leads to an effective replacement of TBA^+ counter charges by H^+, which will eventually lead to precipitation of an amorphous form of HTO or HTO-like material.

3.5. Relationship between Interlayer Spacing and Debye Length. In a series of experiments in which the concentration of TBA^+ in solution was varied by dilution with water at constant TBA/HTO ratio, a linear relationship was observed between $1/d^2$ and the TBA^+ concentration, as shown in Figure 6 (samples D0−D4). In this representation, complete exfoliation may be defined by the condition $1/d^2 = 0$. Extrapolation of the experimental curve in Figure 6 to lower TBA^+ concentration indicates that this condition is met when $C_{TBA} = 12.7$ mmol/L. Because TBA/HTO was 3.7, this implies that a completely exfoliated nanosheet solution has an equivalent HTO concentration of 3.4 mmol/L or lower under these conditions.

The observed trend in Figure 6 is suggestive of a correlation between the interlayer distance d and the ionic strength I of the solution, which is related to the Debye screening length κ^{-1} via

$$\kappa^{-1} = \sqrt{\frac{\varepsilon k_B T}{2 N_A e^2 I}} \qquad (4)$$

Here, ε is the permittivity of the solvent, k_B is the Boltzmann constant, T is the temperature, N_A is the Avogadro constant, and e is the elementary electron charge. The ionic strength I is defined as $I = 1/2\sum c_j z_j^2$, where c_j and z_j are the concentration and ionic charge, respectively, of ions of type j. Because the TBA/HTO ratio was kept constant in these experiments, the ionic strength is proportional to C_{TBA}. Also because I is also proportional to κ^2, C_{TBA} is proportional to κ^2. If the interlayer distance would be solely determined by the electrical double layer, the parameter $1/d^2$ would be proportional to the TBA^+ concentration. This is not the case because the trend in Figure 6 does not cross the X-axis at $C_{TBA} = 0$. Nevertheless, the linear trend in this graph clearly suggests a substantial influence of

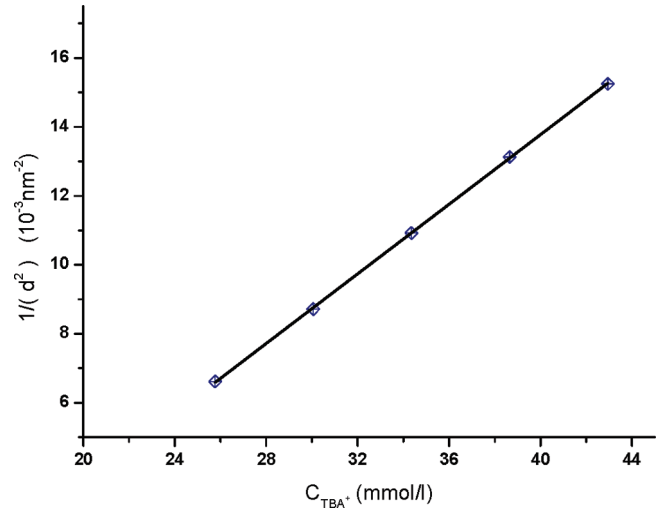

Figure 6. Reciprocal square of interlayer distance ($1/d^2$) versus TBA^+ concentration c_{TBA} at a constant TBA/HTO ratio of 3.7.

the electrical double layer, characterized by the Debye screening length κ^{-1}, on the interlayer spacing d.

In the experiments reported in Figure 6, the ionic strength I is in the range between 37 and 63 mmol/L, which corresponds with a Debye screening length κ^{-1} of 1.57 and 1.22 nm, respectively, that is, a variation of 29%. In the same series of experiments, the d-spacing decreased by about 50%, which is of similar order of magnitude as the reduction of Debye length. When we assume that electrostatic interactions between nanosheets and oppositely charged counterions play a predominant role in the determination of the interlayer distance d, we can model a stack of nanosheets in terms of the Gouy−Chapman model.[17] In the Gouy−Chapman model, the electrostatic potential (Ψ) at a distance x from a single negatively charged nanosheet with electrostatic surface potential Ψ_0 can be described by eq 5:

$$\Psi(x) = \Psi_0 \cdot \exp(-\kappa \cdot x) \tag{5}$$

In a stack of sheets that are each separated by an interlayer distance d, the electrostatic potential between two sheets can then be described approximately by the sum of the electrostatic potentials of both individual sheets. Thus, we can write:

$$\Psi_{1\leftrightarrow 2}(x) \approx \Psi_1(x) + \Psi_2(d - x) = \Psi_0 \cdot (\exp(-\kappa \cdot x) - \exp(-\kappa \cdot (d - x)))$$

The minimum electrical potential occurs exactly in the midpoint between two sheets at $x = d/2$. The potential $\Psi_{1\langle - \rangle 2}$ ($d/2$) at that location is about 7% of the potential at the surface of a single sheet (Ψ_0). This shows that the electrostatic interaction of the diffuse double layer spans the width between restacked nanosheets. We may conclude that the titania nanosheets within the stacks are most likely organized and separated by a diffuse layer of predominantly positively charged ions instead of the well-defined ionic bonds that were present in the original lepidocrocite $HTi_{1.6}O_{3.7} \cdot H_2O$ and $K_{0.8}Li_{0.27}Ti_{1.73}O_4$ structures.[11]

4. Conclusions

The Fluctuating Gap Model was able to provide a good description of the experimental data. The model is a useful tool for the determination of the interlayer distance d between sheets, the average stack size $\langle m \rangle$, and the fraction of nanosheets in solution x from experimental SAXS data of titania nanosheet solutions. The exfoliation of a protonated layered titanate crystal and the restacking of exfoliated anionic nanosheets in the presence of TBA^+ ions were found to be a dynamic process that was sensitive to both the concentration and the molar ratio of TBA^+ and H^+ ions. However, within certain limits, the interlayer distance d and stack size $\langle m \rangle$ could be changed reversibly upon addition of TBAOH or nitric acid. We also found that the interlayer distance d between (re)stacked nanosheets is roughly proportional to the Debye screening length of the solution. According to the Gouy−Chapman model, the electrostatic potential will decrease by 93% from the surface of a sheet to a location in solution exactly between two sheets. The negatively charged nanosheets are therefore most likely separated by a diffusive layer of positively charged ions.

Acknowledgment. This work was financially supported by the Chemical Sciences division of The Netherlands Organization for Scientific Research (NWO-CW). We thank The Netherlands Organization for Scientific Research (NWO) for beam time at the ESRF DUBBLE beamline. We thank Dr. G. Portale and Dr. W. Bras from DUBBLE for on-site assistance and useful discussions.

Supporting Information Available: Validation of the parameters used in the Fluctuating Gap Model. This material is available free of charge via the Internet at http://pubs.acs.org.

References and Notes

(1) Sasaki, T. *J. Ceram. Soc. Jpn.* **2007**, *115*, 9–16.
(2) Osada, M.; Sasaki, T. *J. Mater. Chem.* **2009**, *19*, 2503–2511.
(3) Geim, A. K. *Science* **2009**, *324*, 1530–1534.
(4) Sasaki, T.; Watanabe, M.; Hashizume, H.; Yamada, H.; Nakazawa, H. *J. Am. Chem. Soc.* **1996**, *118*, 8329–8335.
(5) Osada, M.; Akasuka, K.; Ebina, Y.; Funakubo, H.; Kiguchi, T.; Takada, K.; Sasaki, T. *Jpn. Soc. Appl. Phys.* **2007**, *46*, 6979–6983.
(6) Osada, M.; Ebina, Y.; Funakubo, H.; Yokoyama, S.; Kiguchi, T.; Takada, K.; Sasaki, T. *Chem. Mater.* **2006**, *18*, 1023–1027.
(7) Osada, M.; Ebina, Y.; Fukuda, K.; Ono, K.; Tanaka, K.; Yamaura, K.; Takayama-Muromachi, E.; Sasaki, T. *Phys. Rev. B* **2006**, *73*, 153301.
(8) Sato, H.; Okamoto, K.; Tamura, K.; Yamada, H.; Sarywatari, K.; Kogure, T.; Yamagishi, A. *Appl. Phys. Express* **2008**, *1*, 035001.
(9) Sasaki, T.; Watanabe, M. *J. Am. Chem. Soc.* **1998**, *120*, 4682–4689.
(10) Sasaki, T.; Kooli, F.; Iida, M.; Michiue, Y.; Takenouchi, S.; Yajima, Y.; Izumi, F.; Chakoumakos, B. C.; Watanabe, M. *Chem. Mater.* **1998**, *10*, 4123–4128.
(11) Tanaka, T.; Ebina, Y.; Takada, K.; Kurashima, K.; Sasaki, T. *Chem. Mater.* **2003**, *15*, 3564.
(12) Sasaki, T.; Ebina, Y.; Tanaka, T.; Harada, M.; Watanabe, W. *Chem. Mater.* **2001**, *13*, 4661–4667.
(13) Pizzey, C.; Klein, S.; Leach, E.; van Duijneveldt, J. S.; Richardson, R. M. *J. Phys.: Condens. Matter* **2004**, *16*, 2479–2495.
(14) Bras, W.; Dolbnya, I. P.; Detollenaere, D.; van Tol, R.; Malfois, M.; Greaves, G. N.; Ryan, A. J.; Heeley, E. *J. Appl. Crystallogr.* **2003**, *36*, 791–794.
(15) Bras, W.; Emsley, J. W.; Levine, Y. K.; Luckhurst, G. R.; Seddon, J. M.; Timini, B. A. *J. Phys. Chem.* **2004**, *121*, 4497–4513.
(16) Hosemann, R.; Bagchi, S. N. *Direct Analysis of Diffraction by Matter*; North-Holland Publishing Co.: Amsterdam, 1962; pp 409−419.
(17) Barnes, G. T.; Gentle, I. R. *Interfacial Science*; Oxford University Press: Oxford, 2005; pp 195−197.

JP108687Q